

Development of Aluminum-Lithium Alloys[†]

Z. Q. Hu, Y. Y. Li, Y. Zhang, D. P. Yao, X. J. Jiang

Institute of Metal Research, Academia Sinica 72 Wenhua Ave., Shenyang 110015, China

Abstract: The extensive investigation of aluminum-lithium alloys in the last decade has been driven largely by numerous potential structural application in the aerospace industry requiring a low density metallic material having good strength-toughness combination and high stiffness. There has also been increasing interest in the cryogenic properties of these alloys. IMRAS puts great effort focused on the frontier of development of new materials, and Al-Li alloys is one of them. A brief review of the recent results in the research of Al-Li alloys in IMRAS is compiled, including the role of δ' phase, the PFZ formation, the behaviors of alloying elements, the mechanical properties both at room and cryogenic temperatures, the effect of rapid solidification etc.

1 Introduction

Al-Li alloys are extremely attractive to designers due to their lower density and higher elastic modulus than conventional Al alloys with similar combinations of mechanical properties^[1], that is why we have to put emphasis to study this new Al-Li alloys in order to meet the needs of the high tech and economic development.

Al-Li alloys are very attractive candidates of structural materials for aviation and aerospace applications. In early stage, the application was limited because of low ductility.

Nowadays, great progress has been achieved on the research of improving their low ductility^[2-5].

Recently, Al-Li alloys were also found to have novel properties even at cryogenic temperatures, i. e., the strength, the ductility and the fracture toughness are all improved with decreasing test temperature^[6-17].

On the basis of the understanding of Al-Li alloys, a series of Al-Li alloys have been developed and selected to be used in the designing of new aeroplanes. The future prospect of Al-Li alloys is hopeful. Of course, more research works are necessary in order to know deeper and better.

2 Role of δ Phase

The metastable δ' (Al_3Li) phase in the Al-Li system has recently attracted significant interest because of its role as a main hardening precipitate, which has a Li_2 type superlattice

[†]本文原载于《THE CHALLENGES TO ADVANCED NEW MATERIALS》, Korea, 1990, 121-145.

structure. The non-optimal deformation and fracture behavior of Al-Li alloys has been attributed in part to the strain localization that results from the planar slip of shearable δ' precipitates. Therefore it is necessary to know more about the δ' phase.

The hardness of Al-2.45wt% Li alloy depends on both aging temperature and time(Fig. 1), which influence the δ' particle size and amount remarkably, that can be quantitatively expressed with a following equation^[18].

$$a = 1 - \exp(-kt^n) \quad (1)$$

where a is volume fraction of δ' phase, t is ageing time, k and n are the constants.

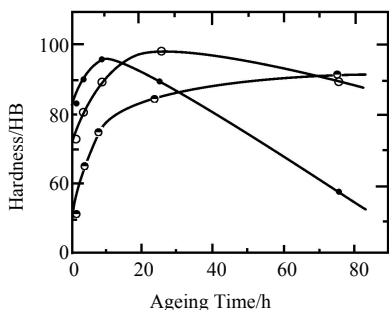


Fig. 1 The hardness at different ageing temperatures for various times^[18]

● 160°C; ○ 190°C; ● 229°C

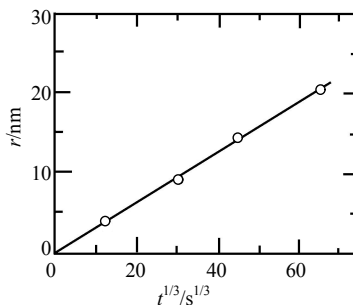


Fig. 2 The average radius of δ' particle vs. aging time at 190°C^[18]

The δ' coarsening related to aging time is obeyed the Lifshitz-Slyozov-Wagner theory, showing that the average radius of δ' particles increase with one third root of time, as shown in Fig. 2. From the relationship between the aging temperature and average radius of δ' particles, Following Bulmuth's equation^[19], the activation energy for δ' coarsening is 133.7kJ/mol, 131.1kJ/mol, and 123.6kJ/mol for aging time of 5h, 8h and 25h respectively, and they are approximately the same as the activation energy for lithium atom diffusion as 126.1 ± 5.2 kJ/mol at temperature between 423~513K^[20].

It can be clearly concluded that the mechanism of δ' coarsening is diffusion-controlled.

Al-2.29Li-3.65Zn-0.08Zr(wt%)alloy also obeys the same rule^[21], as shown in Fig. 3.

The δ' precipitation is also influenced by the quenching rate and cold deformation, because both of them change the vacancy concentration and dislocation density. The results prove that the higher the concentration of vacancy, the faster the δ' coarsening, the wider the PFZ at grain boundary. The cold deformation prior to aging enhances high density of dislocation in the matrix, which in turn makes the diffusion of lithium atoms easier in Al-2.45wt %Li alloy and accelerates the coarsening rate of δ' phase, as shown in Fig. 4, 5, 6, 7^[22]. Because of the large binding energy of lithium atom with vacancy^[23], it is easy to form a lithium atom-vacancy complex. During the aging, such complexes move to the grain boundary that makes the lithium concentration high there. Finally it forms an equilibrium δ' phase at

grain boundary and a δ' precipitate free zone near the grain boundary.

Study of PFZ formation and growth in Al-11.9at%Li at 463K indicates that they are closely related to aging time (Fig. 8), which depends on the long-range diffusion of lithium atoms^[24]. The particle size of θ' phase becomes smaller near the PFZ interface, and thereafter, it consists of lithium-rich supersaturated solid solution in the PFZ. The half-width of PFZ (W) varies with the square root of aging time, and it can be calculated by the equation.

$$W = kt^{1/2} \quad (2)$$

$$K = 2D^{1/2}(C-C_\alpha)/(C_x-C_\alpha) \quad (3)$$

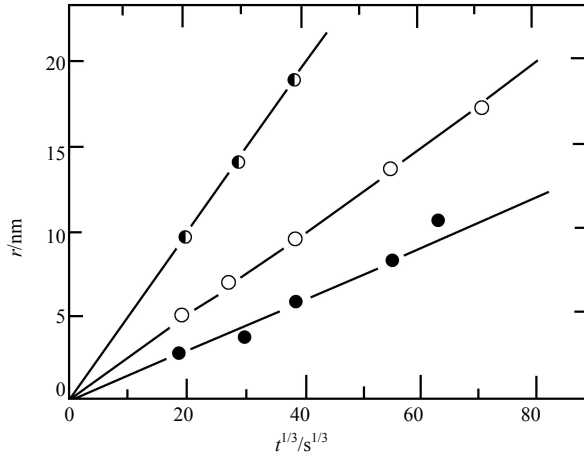


Fig. 3 Relation between the average radius of δ' particles and aging time (Al-2.29Li-3.65Zn-0.08Zr alloy)^[21]

●433K; ○463K; ◐493K

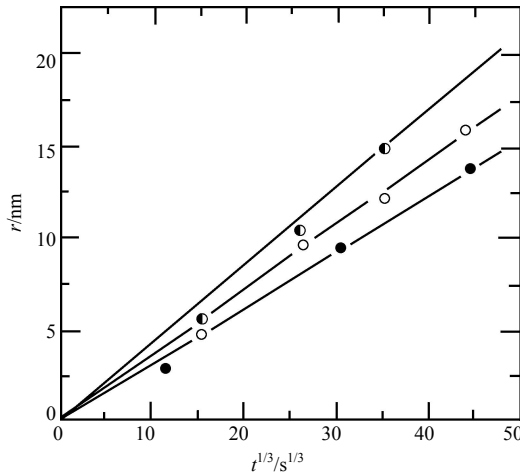


Fig. 4 The effect of deformation prior to aging on the coarsening of δ' phase^[22]

●undeformation; ○10% deformation; ◐20% deformation

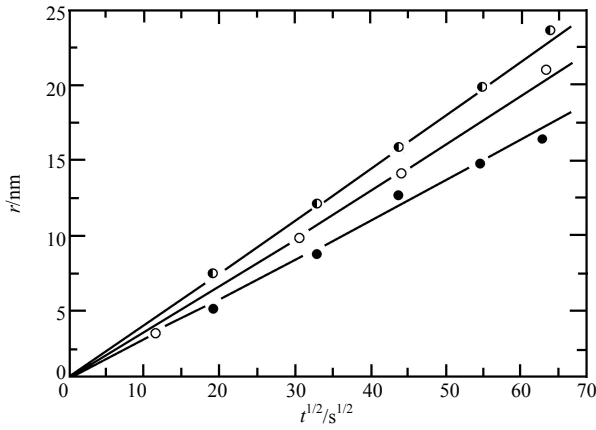


Fig. 5 The average radii of δ ' particles vs. aging times at different quenching rates^[22]

● Quenched in cold salt water; ○ Quenched in cold water; ● Cooled in air

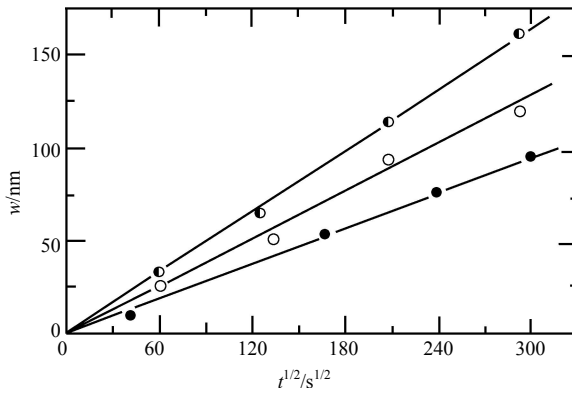


Fig. 6 The half-width of PFZ at grain boundary vs. aging time at the different amounts of deformation^[22]

● undeformation; ○ 10% deformation; ● 20% deformation

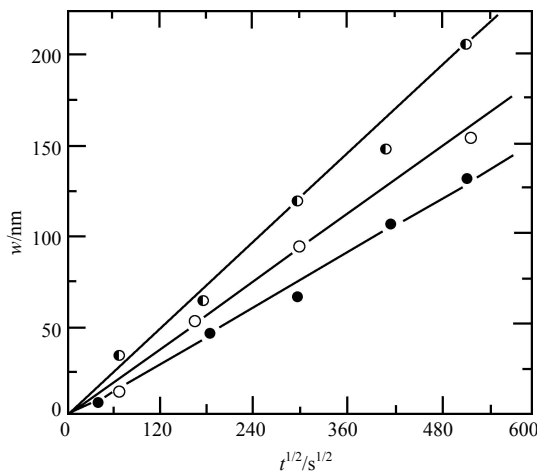


Fig. 7 Effect of quenching rate on the halfwidth of PFZ at the grain boundary for various aging times^[22]

● Cooled in air; ○ Quenched in cold water; ● Quenched in cold salt water

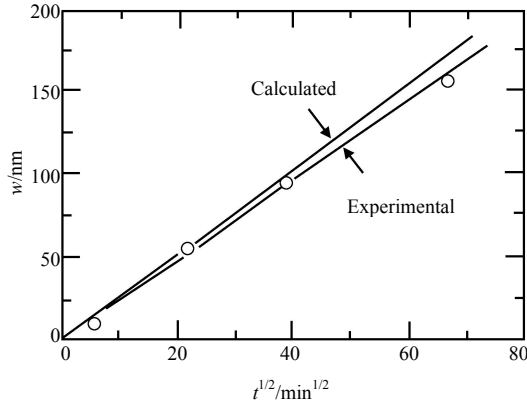


Fig. 8 The PFZ half-Width vs. the square root of aging time in Al-11.9 at % Li^[24]

In Al-11.9at%Li alloy(C), the Li concentration in PFZ(C_x) may be chosen as 26at%(a little larger than 25at% in Al,Li). The Li concentration in the α phase at the PFZ interlace(C_α) is 4.5 at %Li at 463K according to the phase diagram. The diffusion coefficient of Li in α -Al has been Investigated as a function of temperature between 423~513K by Mereau et al. as follow^[20]:

$$D = 0.37[(-126.4 \pm 5.2\text{kJ/mol})RT] \text{ cm}^2/\text{s} \quad (4)$$

Substituting all the above data into eq. (2), we get

$$w = 0.33t^{1/2} \quad (5)$$

The calculated half-width of PFZ related to the square root of aging time is also shown in Fig. 8 which is in good accordance with the measured half-width. Of course, PFZ in Al-Li alloys is still an important task to understand deeply its formation mechanism and to find some measures to eliminate it.

δ' precipitate dissolution in Al-2.45wt%Li alloy is considered to be a thermally activated process. In the case of age-hardening alloys, formation of precipitate phase is exothermic while their dissolution is an endothermic reaction when tested in a differential scanning calorimeter(Fig. 9). The peak A in Fig. 9 represents the dissolution of lithium-rich GP zone.

The dissolution of δ' phase consists of two stages(B_1 and B_2): In the first stage, it needs much larger thermal activation to break down the superlattice structure so as to form a lithium-rich zone. In the second stage, it is the dissolution of this zone. The calculated apparent activation energies are 278.3kJ/mol and 96.1kJ/mol respectively. The latter activation energy is very similar to the activation energy of GP zone determined to be 88.1kJ/mol. It may be postulated the mechanism of the second stage of δ' dissolution is same as that of GP zone dissolution^[25].

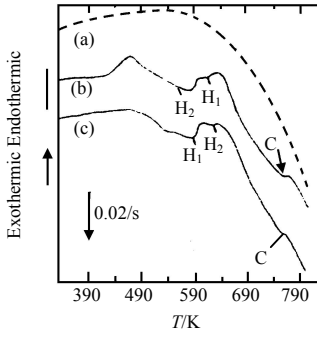


Fig. 9 DSC results from Al-2.45wt%Li alloy at 40K/min^[25]
 (a) vase line; (b) specimen aged at 300K for 2 months(NA);
 (c) specimen aged at 463K for 25h (PA)

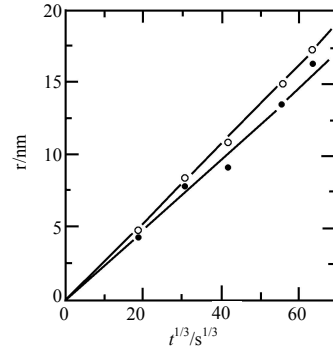


Fig. 10 The mean radii of δ' particles vs. aging time at 463K^[26]
 ● Al-2.91Li-1.01Mg-0.11Zr(wt%);
 ○ Al-2.22Li-2.06Mg-0.15Zr(wt%)

The endothermic peak temperature of δ' dissolution is shown as C in Fig. 9. The δ' phase is very stable in the binary Al-Li alloys.

Therefore its apparent activation energy for lithium to escape from δ' phase is much larger, that was determined to be 565.3kJ/mol (NA) and 536.4kJ/mol(AA)^[25].

3 Functions of Alloying Elements

The magnesium acts as an important solid solution strengthening element, which does not change the tendency of age hardening of Al-Li-Mg-Zr alloy. Mg decreases the Li solubility in the martix. That enhances the coarsening rate of δ' particles, as shown in Fig. 10. The alloy plasticity impairs with the increase of Mg in the alloy, and the elongation is the smallest at peak aging temperature^[26].

The β (Al_3Zr) phase due to the Zr addition can act as the δ' nucleation site and enhance to precipitate T_1 and S phases. If Zr contents in 2090-T6 alloy and 8090-T6 alloy are intentionally lowered to 0.02% and 0.07% respectively. The ultimate tensile strengths are also impaired from 577MPa to 375MPa in the former alloy and from 553MPa to 469MPa in the latter one^[27].

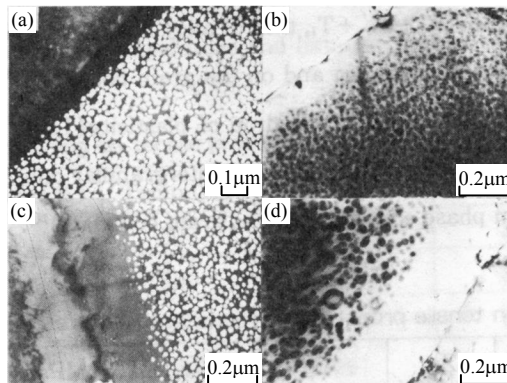


Fig. 11 The PFZ morphology in Al-2.29Li-3.65Zn-0.08Zr alloy aged at 463K
 (a) 6h, (b) 16h, (c) 48h; (d) 100h^[21]

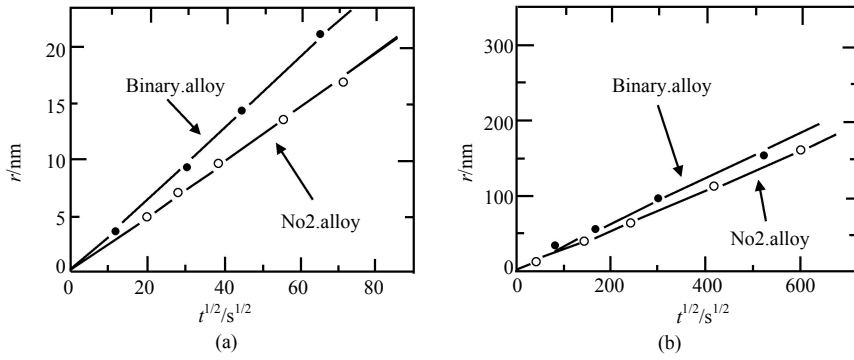


Fig. 12 Relation between aging time and δ' particle size (a) as well as half-width of PFZ; (b) in Al-2.29Li-3.65Zn-0.08Zr alloy aged at 463K^[21]

Zn in Al-Li alloys plays the role of solid solution strengthening, lowers the solid solubility of Li in matrix and retards the growth of δ' phase and PFZ^[21]. Fig. 11 is the PFZ morphology in Al-2.29Li-3.65Zn-0.08Zr(wt%) alloy when aging at various times at 463K.

The longer the aging time, the wider the PFZ. It can be clearly seen that the δ particles are smaller near the PFZ. Fig. 12 shows the relationship of δ' particle size (Fig. 12(a)) and half-width of PFZ (Fig. 12(b)) with aging time.

The microstructure and properties of three kinds of Al-Li-Cu-Zr alloys with Cu/Li ratios of 0.47, 1.17 and 2.39 have been studied. The T_1 platelets grow up during the dissolution of δ' particles, which become smaller and gradually disappear. The sequence of phase precipitation of alloy 1 and alloy 2 is $\delta' \rightarrow \delta' + T_1$ that of alloy 3 is $\delta' + T_1 \rightarrow \delta' + T_1 + \theta'$.

T_1 phase precipitates both in the grain and on the grain boundary^[28]. The tensile strength rises with the increase of Cu/Li ratio and a drop of plasticity (Table 1), accompanying the change of crack mode from transgranular mode to intergranular one, which is caused by the precipitation of equilibrium phase containing Cu at grain boundary^[28].

Table 1 Influence of Cu on tensile properties at room temperature (PA)

Alloy	Li	Cu	Zr	Al	Cu/Li	UTS/MPa	0.2YS/MPa	EL/%
1	2.32	1.09	0.14	bal.	0.47	395	324	8.3
2	2.32	2.62	0.16	bal.	1.17	428	347	7.0
3	2.05	4.90	0.13	bal.	2.39	513	435	5.5

Addition of rare earth element (0.3wt%) to 2090 alloy can refine δ' phase, suppress its growth, enhance strength (Fig. 13) and increase the oxidation resistance^[29]. After oxidation, the surface of 2090 alloy contains more Si, Mg and Li, while the oxide film of 2090RE alloy contains rare earth elements and less Si, Mg and Li, as shown in Fig. 14. That is to say, rare earth elements do not reduce oxidation weight gain, but are substituted for Li and Mg to be oxidized, that induces the reduction of Li and Mg surface depletion of alloys. The widths of surface depletion layer of 2090 and 2090RE alloys after solution treatment at 530 °C for 3h are

shown in Fig. 15. The width of the latter is nearly two third of the former.

4 Enhancement of Cryogenic Mechanical Properties

Recently Al-Li alloys have been proved to be attractive for their enhanced mechanical properties even at cryogenic temperatures. It is a promising candidate in cryogenic aero-space applications such as hydrogen and oxygen fuel tanks in future aerovehicles.

In Al-Li-Zn-Zr alloys, the tensile strength and elongation are increased with decreasing temperature tested down to 17K as shown in Fig. 16^[21], but the elongation of OA specimen has a little drop(Fig. 17)^[30]. The influence of stretching prior aging on tensile properties of Al-Li-Zn-Zr alloys are listed in Table 2. Besides Al-2.75wt%Li, Al-Li-Mg-Zr, Al-Li-Gu-Zr and Al-Li-Mg-Cu-Zr alloys have also been studied. The tensile strength and elongation are also enhanced at liquid nitrogen temperature and listed in Table 3.

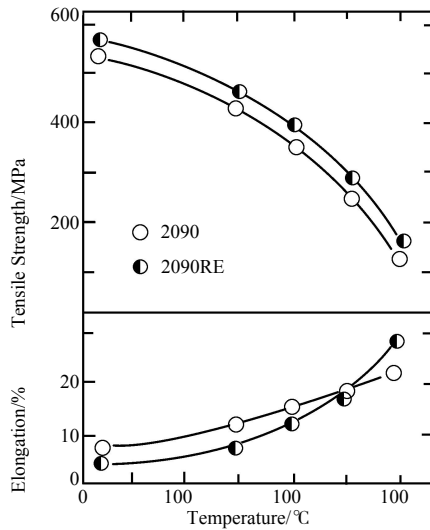


Fig.13 Elevated temperature strength and ductility of both alloys^[29]

Table 2 Influence of stretching on tensile properties of Al-Li-Zn-Zr alloys^[21]

Alloy	Stretching/%	Temp./K	0.2YS/MPa	UTS/MPa	EL/%
1	0	300	240	306	9.7
1	2	300	255	315	7.7
1	5	300	261	315	7.6
2	0	300	251	367	12.0
2	2	300	277	370	8.4
2	5	300	287	381	8.4
1	0	77	244	386	24.1
1	2	77	257	388	20.8
1	5	77	266	390	20.2
2	0	77	254	414	16.0
2	2	77	263	414	11.3
2	5	77	289	437	11.5

Note: Alloy 1-Al-1.80Li-1.02Zn, 789K/lhWQ + 403K/48h

Alloy 2-Al-2.29Li-3.65Zn-0.08Zr, 789K/lhWQ + 433K/16h

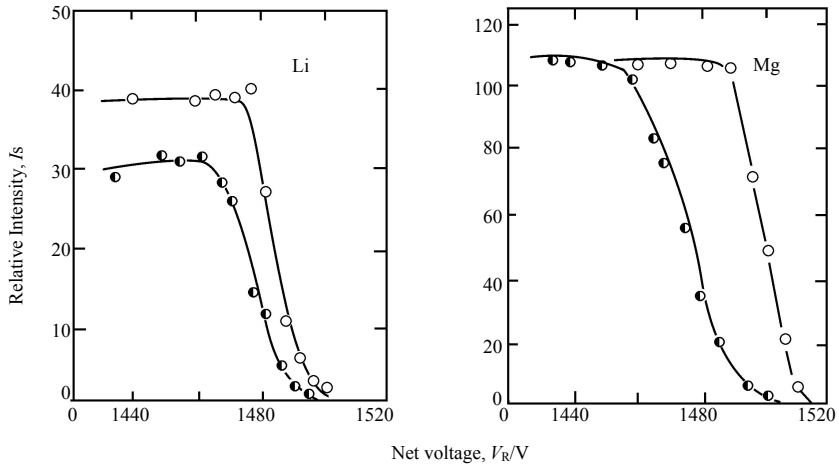


Fig. 14 Effect of 0.3pct mischmetal addition on relative intensity of secondary Li and Mg ion beam^[29]
○2090; ●2090RE

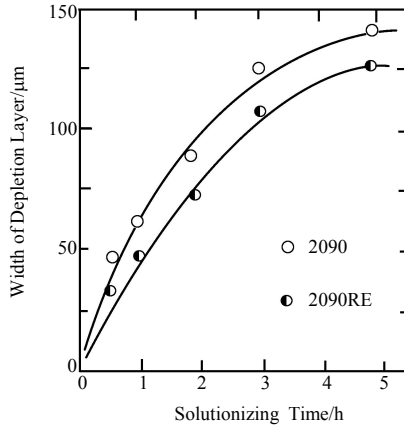


Fig. 15 Influence of solutionizing time on width of depletion layer at 530°C^[29]

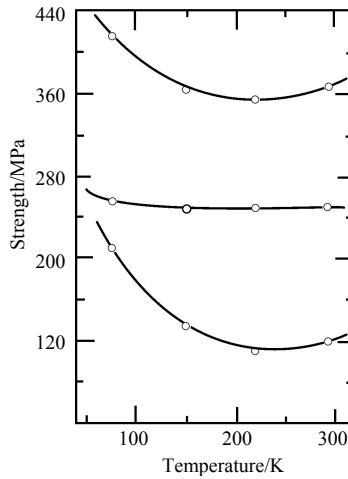


Fig.16 Tensile property of Al-2.29Li-3.65Zn-0.08Zr(wt%) alloy at cryogenic temperatures^[21]

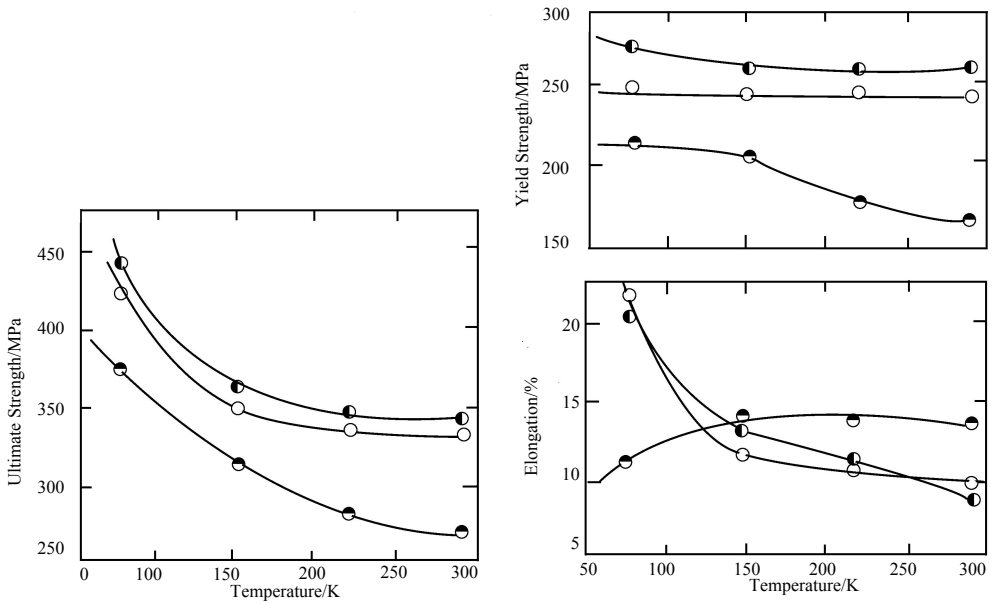


Fig.17 Tensile properties of Al-Li-Mg-Zr alloy vs. test temperature^[30]

○ UA; ◐ PA; ● OA

Table 3 Ratios of mechanical properties of Al-Li alloys tested at cryogenic temperature compared to those tested at room temperature

Alloy	Treatment Condition	Temp./K	UTS	YS	EL	K _{ic}	Ref.
2090	T6	77	1.27	1.17	1.77	1.58	[14]
2090	T8	77	1.21	1.09	1.45		[31, 32]
2090	T8	4	1.39	1.11	1.88		[31, 32]
2090	T8E41	77	1.27	1.12	1.27	1.42	[12, 33]
2090	T8E41	4	1.45	1.15	1.64	1.78	[12, 33]
2091	T351	77	1.32	1.20	1.60	1.24	[31]
2091	T8	77	1.18	1.13	1.67	1.33	[31]

Alloy	Treatment Condition	Temp./K	UTS	YS	EL	K _{ic}	Ref.
2091	T8	4	1.31	1.25	1.40	1.33	[31]
2091	T8X	77	1.27	1.20	1.60	1.24	[33]
8090	T351	77	1.24	1.13	1.41	0.74	[13,17,33]
8090	T651	77	1.25	1.06	1.67		[13,17,33]
8091	T351	77	1.37	1.24	1.27	0.74	[33]
8091	T351	77	1.20	1.07	2.00	1.90	[33]
Al-0.93Li	T8X	77	1.99	1.13	1.16		[34]
Al-2.45Li	T6	77	1.21	1.11	1.05		[34]
Al-2.75Li	T6	77	1.12	1.04	1.50		[35]
Al-2.29Li-3.65Zn-0.08Zr	T6	77	1.26	0.01	2.48		[21]
Al-2.29Li-3.65Zn-0.08Zr	T6	77	1.13	0.01	1.33		[21]
Al-2.32Li-1.09Cu-0.14Zr	T6	77	1.28	1.06	1.83		[36]
Al-2.23Li-2.62Cu-0.16Zr	T6	77	1.21	1.09	2.14		[36]
Al-2.05Li-4.90Cu-0.13Zr	T6	77	1.01	0.91	2.33		[36]
Al-2.19Li-1.01Mg-0.11Zr	T6	77	1.25	1.05	3.00		[30]
Al-2.22Li-2.06Mg-0.15Zr	T6	77	1.22	1.03	1.64		[37]

The ultimate tensile strength is generally associated with the strain hardening behavior of a metal, and its increase at cryogenic temperature may be attributed to the improving of strain hardening ability. It can also be understood that the strengthening of δ' phase is the most outstanding factor at low temperatures. The ordered nature of δ' phase causes the dislocations to move in pairs during plastic deformation. The antiphase domain energy of the δ' phase is increased so that it is difficult to result in its cutting by dislocation pairs at low temperatures, which can partly account for a more homogeneous deformation mode(Fig. 18(b)), compared with the planar slip deformation mode occurred at room temperature(Fig. 18(a)). A more homogeneous slip distribution and dispersed strain localization at cryogenic temperatures leads to a higher ductility^[21].

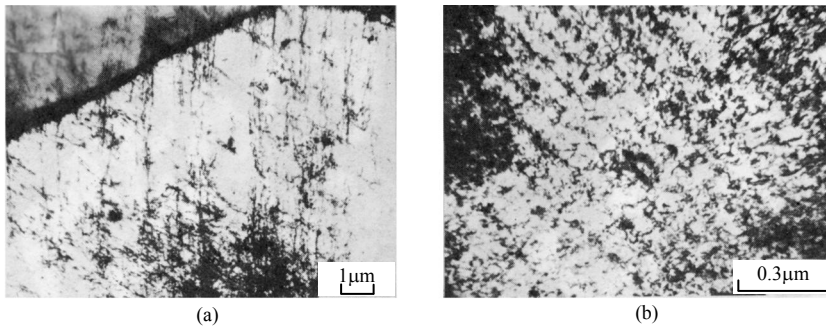


Fig. 18 Dislocation structure near the tensile fracture of Al-2.29Li-3.65Zn-0.08Zr(wt%) alloy at room temperature(a) and 77K(b)^[21]

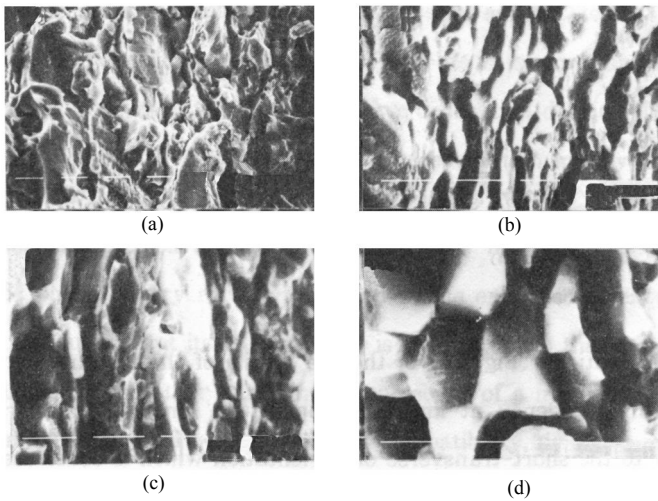


Fig. 19 Tensile fracture morphology of Al-2.29Li-3.65Zn-0.08Zr(wt%) alloy at 295K (a)、220K (b)、150K (c)、77K^[21](d)

Fig. 19 shows the cracking appears transgranular mainly at room temperature, and changes to an intergranular mode chiefly at 77K. The failure of Al-Li alloys may be contributed in part to the interaction between the grain boundary precipitates and the slip bands. Because of the increase of matrix strength of Al-Li alloys relative to the grain boundary at cryogenic temperatures, large amount of dislocation pile up at grain boundaries, nucleate microcracks there and propagate along the grain boundary, resulting in the trend of intergranular fracture.

Optical microscopy observations (Fig. 20) of the profile of the fracture surfaces indicate that there is an increasing tendency at low temperature for intergranular delamination (splitting) perpendicular to the short-transverse orientation which is considered as a reason for the improvement of ductility of Al-Li alloys at cryogenic temperature. However it still remains a question of how to explain there is no enhancement of ductility at over-aged condition despite of many intergranular delaminations on fracture surface.

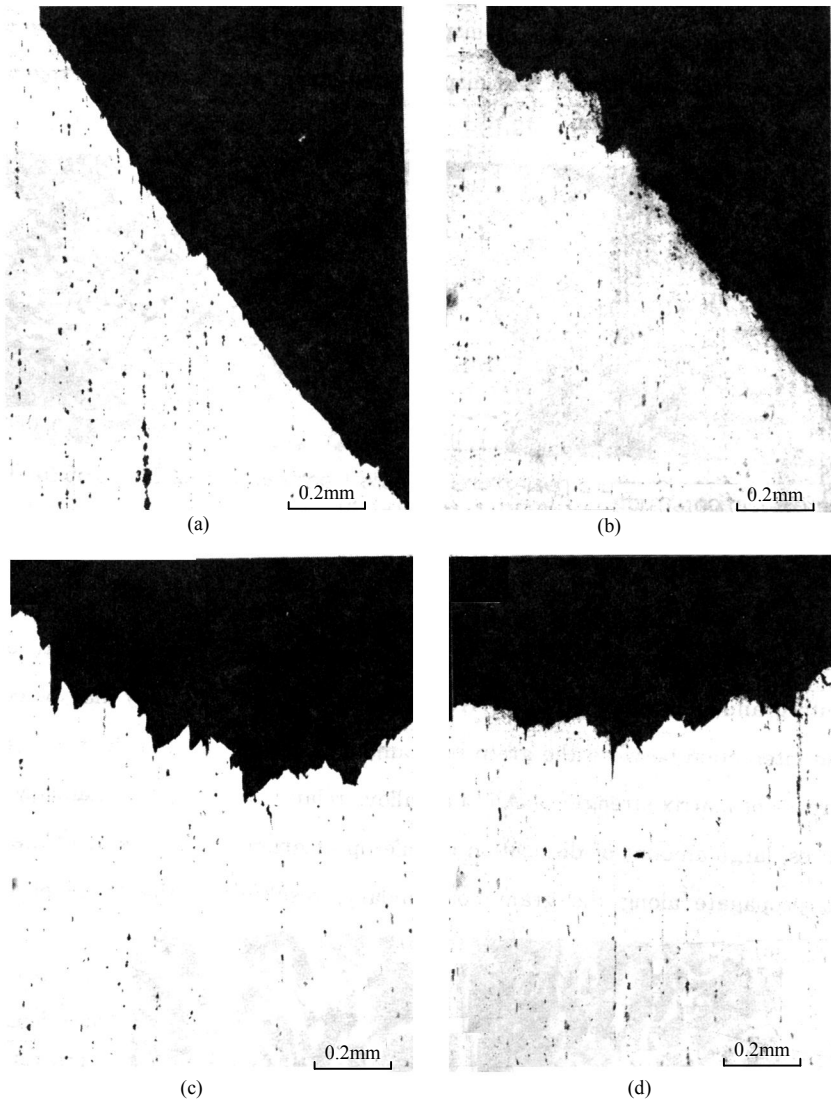


Fig. 20 Lateral view of tensile fracture of Al-2.29Li-3.65Zn-0.08Zr(wt%) alloy at 295K (a), 220K(b), 150K(c) and 77K(d)^[21]

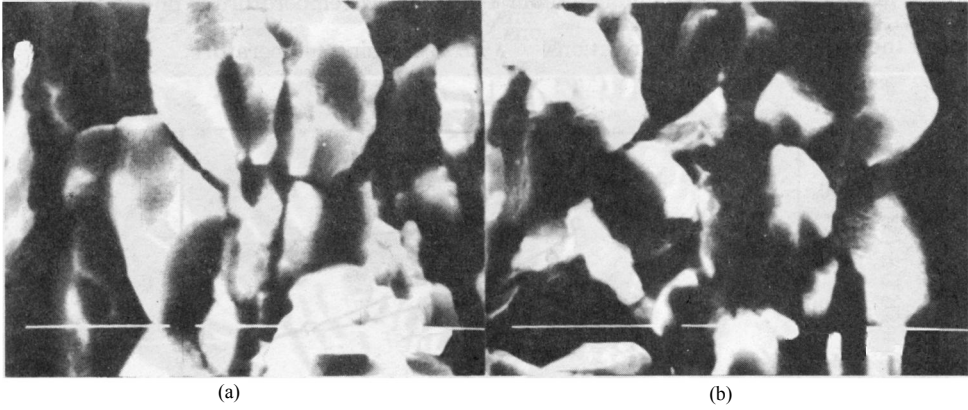


Fig. 21 Tensile fracture morphology of Al-2.29Li-3.65Zn-0.08Zr(wt%) alloy after stretching tested at 77K^[21]
 (a) 2% stretching; (b) 5% stretching

The influence of stretching prior aging on tensile properties of Al-Li-Zn-Zr alloys seems to increase the strength and decrease the ductility both a little bit. The fracture mode at cryogenic temperatures after stretching are the same as that tested without stretching, as shown in Fig. 21. It means the tensile fracture mode is same and stretching has no pronounced effect on it. Stretching creates a high dislocation density. The higher the deformation, the more the dislocation. Because the δ' precipitation mainly depends on the vacancy concentration and Li diffusion in matrix as already mentioned before, the nucleation and growth of the δ' phase is very rapid. However, the existence of enormous dislocations can accelerate the Li diffusion, but its influence is still not much that makes the strength of Al-Li alloys rise a little. On the other hand, the presence of a large amount of dislocation kinks lowers the strain hardening ability and grain compatibility, that impairs the ductility.

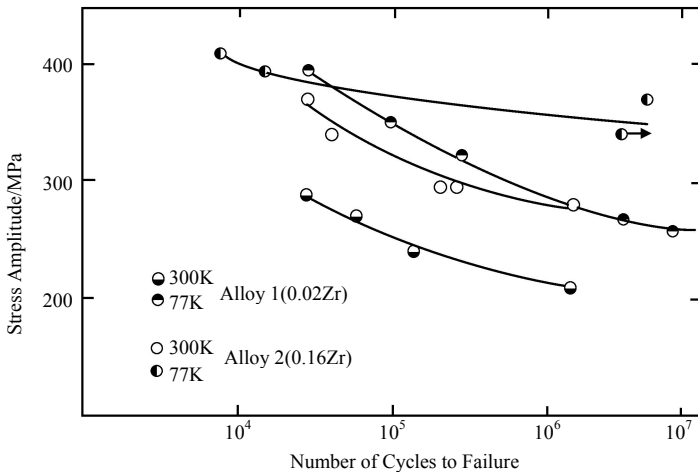


Fig. 22 S-N curves of the alloys fatigued at 300K and 77K^[38]

5 Fatigue and Fracture Mode

It is generally accepted that good high cycle fatigue properties are associated with high yield strength, but ductility plays a more important role in low cycle fatigue. Obviously, the increase in fatigue life of aluminum-lithium alloys at low temperature is due to the improvement in the strength-toughness relationship with decreasing temperature.

The fatigue property of alloy 1 (Al-2.85Cu-1.88Li-0.22Mg-0.02Zr) and alloy 2 (Al-2.88Cu-2.30Li-0.23Mg-0.17Zr) has been studied. The fatigue specimens were taken from the plate of 4.5mm thickness in L/T orientation. Specimens of both alloys were solutionized at 515 °C for 2 hours, quenched in iced water and aged for 24 hours at 165 °C to develop a peak precipitation hardening (T6). Fatigue tests were conducted on a Schenck servo-hydraulic machine at both room temperature (300K) and liquid nitrogen (77K). The S-N curves are shown in Fig. 22. It is noted that the addition of Zr can increase the room temperature fatigue strength significantly over the whole range of fatigue life. However, Zr addition has less effect on the high stress fatigue life at low temperature^[38].

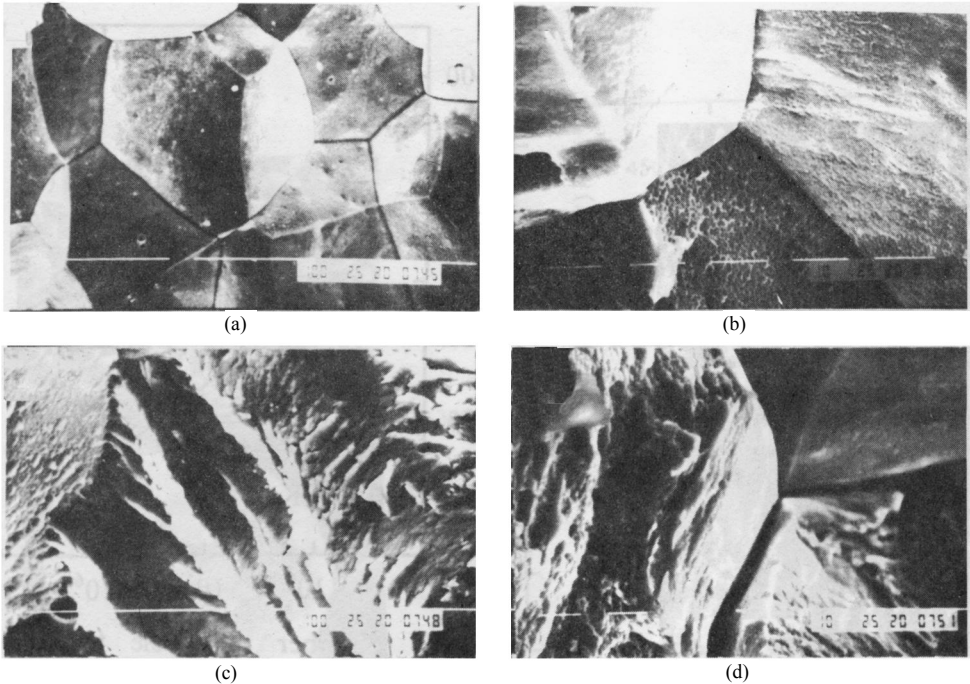


Fig. 23 Fracture surfaces of alloy 1 fatigued at 300K(a) (c) and 17K(b) (d)^[38]

Fig. 23 illustrates the fatigue fracture surfaces of alloy 1 at room temperature and liquid nitrogen temperature, which demonstrate an intergranular fatigue failure with numerous microvoid dimples on grain boundary, indicating a typical grain boundary ductile fracture which is often found in precipitation hardened aluminum alloy at low temperature^[39].

As mentioned above, Zr addition enhances the ultimate tensile strength, yield strength and ductility, that in turn is correlated to the improvement of the fatigue strength. However, the mechanism responsible for the variation in fatigue property with temperature is not currently well understood. One explanation for a higher toughness at low temperature involves the immobilization of low melting point impurities that are segregated at grain boundary^[11].

Careful AES analysis on a grain boundary fracture surface was done in the present study and indicate no low melting point impurities, such as K and Na at the grain boundaries.

The fatigue strength has been found to increase with drop of temperature. It is considered to associate with the change in the fracture mode. According to the observation, the improvement of strength at 77K might be attributed to the deeper and larger delamination occurred on the fracture mode(Fig. 24).

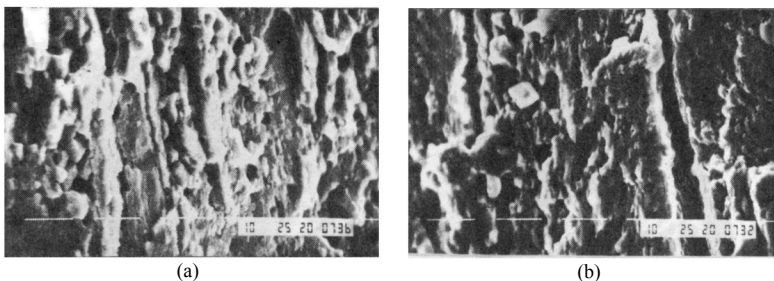


Fig. 24 tractographs of alloy 2 fatigued at 300K (a)、77K^[38] (b)

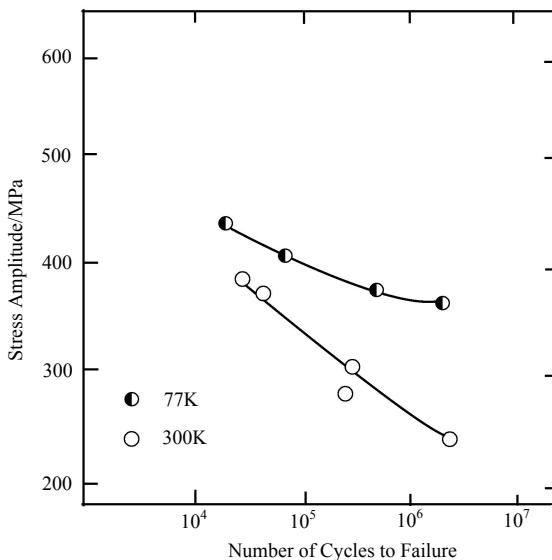


Fig. 25 S-N curves of the alloy fatigued at 300K and 77K^[40]

Fig. 25 is the S-N curves of 8090-T6 alloy fatigued at 300K and 77K. The fatigue life at 77K is much longer than that tested at 300K^[40].

The fracture mechanism at cryogenic temperature of 8090-T6 alloy is the same as that of 2090 alloy, also exhibiting deeper and larger number of delaminations which seems to disperse

the strain concentration leading to the shear deformation localization.

In this research field, the various fatigue mode should be continued to be studied, such as HCF and LCF with long and short cracks, corrosion fatigue in order to have a clear understanding to guarantee the safety service.

6 Rapid Solidification of Al-Li Alloys

The microcrystalline powders of Al-2.90Li-0.84Cu-0.5Mg-0.61Zr alloy was produced by ultrasonic atomization in an argon atmosphere. The cooling rate is about 10^5K/s . Fig. 26 is the micrographs of the ultrasonic gas atomized powders^[41].

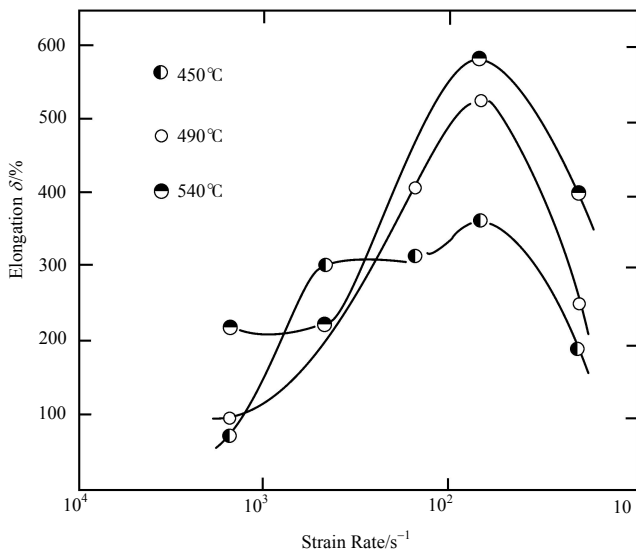
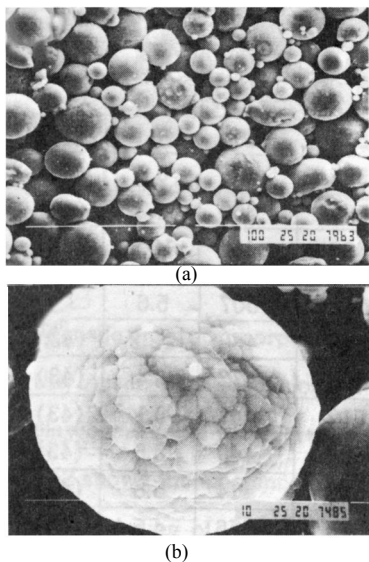


Fig. 26 Micrographs of the ultrasonic gas atomized powders^[41]

Fig. 27 Influence of strain rate on elongation of alloy 1 at constant temperature^[42]

The cellular structure was found in the atomized powders. The width of cells in particles with diameter of $30\mu\text{m}$ is about $1.5\mu\text{m}$. The Al-Li alloys produced by P/M process has refined microstructure with low segregation and possesses higher ductility. The influence of strain rate on elongation at constant temperature has been investigated(Fig. 27). For example, at the condition of strain rate $1.67 \times 10^{-2}\text{s}^{-1}$, the maximum elongations tested at $450\text{ }^\circ\text{C}$ are $490\text{ }^\circ\text{C}$ and $540\text{ }^\circ\text{C}$ are 360% , 525% and 585% respectively. The amount of cavities is increased with the extension of elongation^[42].

Alloy A (Al-2.24Li-1.48Cu-1.20Mg-0.26Zr) and alloy B(Al-3.51Li-1.08Cu-0.63Mg-0.37Zr) were produced by rapid solidification of ultrasonic atomization and liquid dynamic compaction (LDC). Fig. 28 shows the equiaxed grain size of $30\sim 40\mu\text{m}$. The deposited alloys were further densified by hot rolling or hot extrusion. The final grain size was about $2\mu\text{m}$. In comparison with rapidly solidified powder metallurgy alloys(RS-PM), the LDC process has a

higher ductility(Table 4)^[43].

Table 4 Tensile properties of RS Al-Li alloys

Specimen	Solution Temp./K	Aging Temp./K	UTS/MPa	YS/MPa	EL/%	Ref.
Al-2.5Li-4.8Mg-0.1Zr		PA	524	407	3.0	[44]
Al-2Li-3Cu-1Mg-0.2Zr		PA	510	387	15.3	[44]
Al-2Li-3Cu-1Mg-0.2Zr		PA	622	554	10.6	[44]
Al-3.2Li-2.1Cu-1Mg-0.45Zr		PA	525	479	6.0	[45]
8090		PA	507	369	5.2	[46]
A-1	773	443	497	464	10.5	[43]
A-2	773	443	542	507	5.6	[43]
A-1	773	463	516	460	12.2	[43]
A-2	773	463	535	472	6.4	[43]
A-1	793	463	512	447	9.1	[43]
A-2	793	463	503	440	8.5	[43]
B-1	793	463	519	414	5.8	[43]
B-2	793	463	616	558	4.5	[43]
B-3	793	463	499	437	6.1	[43]
B-1	773	443	471	388	6.4	[43]
B-2	773	443	584	557	3.6	[43]
B-3	773	443	544	495	6.8	[43]

Note: A-1-LDC + hot rolling, A-2-RS-PM

B-1-LDC + hot rolling, B-2-LDC + extrusion

B-3-LDC + extrusion + hot rolling

The improvement in ductility may be attributed to a decrease in oxide content of spray deposited alloys.

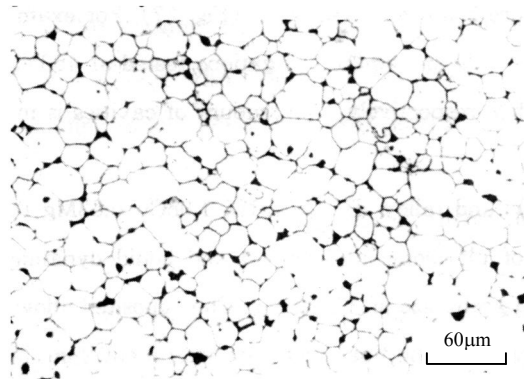


Fig. 28 Equiaxed grain structure of as-deposited alloy A^[43]

The tensile fracture morphology is shown in Fig. 29. Specimen A-1 ruptured at 45 °C Angle with the tensile axis, e. g. along the maximum shear stress direction. Heavy rolling texture may play some role in the formation of such fracture surface. The fracture surface of

specimen A-2 shows the existence of some micropores.

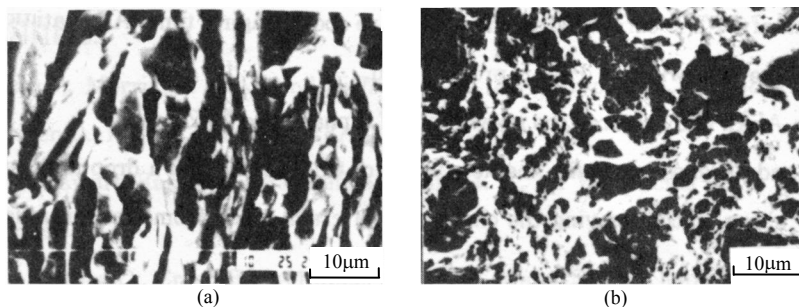


Fig. 29 SEM micrographs of fractured samples of alloy A produced by (a) LDC、(b) RSPM^[43]

The laserglazing of Al-2.23Li-2.62Cu-0.16Zr alloy has been studied by a 2kW CO₂ laser with a cooling rate about 10⁵K/s. The refined grains epitaxially form and their orientation is parallel to the direction of heat flow during cooling. The grain size decreases with the rise of scanning rate^[47]. The fracture mode of laserglazed zone is a transgranular cracking. It forms high concentration of vacancy and high density of dislocation, that make the nucleation sites of metastable precipitates increase. The microhardness of the melted laser irradiated zone (about H.115) is larger than that of the substrate material (about H. 60). After aging, it continues to rise up to about H.145.

Based on the previously obtained results, the study of rapid solidification of Al-Li alloys has a future promising prospect.

7 Conclusions

(1) The mechanism of δ' coarsening is diffusion-controlled. The activation energy for coarsening is approximately the same as the activation energy for lithium atom diffusion.

(2) δ' dissolution consists of two stages: breaking down the superlattice structure to form a lithium-rich zone and finally dissolving this zone.

(3) The half-width of PFZ is correlated to the square root of aging time. A equation for the calculation of the half-width of PFZ is proposed.

(4) Zn addition in Al-Li alloy retards the growth of δ' phase and PFZ.

(5) The strength and hardness rise with the increase of Cu/Li ratio and a drop in plasticity in Al-Li-Cu-Zr alloys, accompanying the change of crack mode from transgranular mode to intergranular one.

(6) An appropriate addition of rare earth element can improve strength and ductility as well as increase the resistance to oxidation.

(7) The enhancement of tensile and fatigue properties can be explained by an increasing tendency of intergranular delamination (splitting) at cryogenic temperatures, that results in the dispersion of strain concentration leading to the shear deformation localization.

(8) Rapid solidification of Al-Li alloys can refine the microstructure, suppress the segregation and improve the ductility. Liquid dynamic compaction is a good consolidation process to be recommended.

(9) Microcrystalline Al-Li alloys possess superplasticity. The maximum elongation at a strain rate of $1.67 \times 10^{-2} \text{s}^{-1}$ reaches 585% tested at 540°C.

References

- [1] Noble B, Harris S J, Dinsdale K. J. *Mater Sci.*, 1982, 17: 461
- [2] Venkateswara Rao K T, Yu W, Ritchie R O. *Scripta Metall.*, 1986, 20: 1459
- [3] Pritchett T R. *Light Metal Ago*, 1986, 44(7/8): 10
- [4] Feng W X, Lin F S, Starke Jr E A. *In: Sanders Jr T H, Starke Jr E A. Aluminum-lithium Alloys II. TMS-AIME, Warrendale, PA, 1983. 17*
- [5] Catalog of Cegedur-Pichiney Co
- [6] Webster D. *In: Baker C, Gregson P J, Harris S J, Peel C J. Aluminum-Lithium Alloys III. The Institute of Metals, London, 1986. 602*
- [7] Dorward R C. *Scripta Metall.* 1986, 20: 1379
- [8] Glazer J, Verzasconi S L, Dalder E N, Yu W, Emigh R A, Ritchie R O, Morris Jr J W. *Adv. Cryo. Eng.*, 1986, 32: 397
- [9] Glazer J, Verzasconi S L, Sawtell R R, Morris Jr J W. *Metall. Trans. A.*, 1978, 18A:1695
- [10] Glazer J, Morris Jr J W, Nieh T G. *Adv. Cryo. Eng.*, 1987, 34: 291
- [11] Webster D. *Metall. Trans. A.*, 1987, 18A: 2181
- [12] Venkateswara Rao K T, Hayashigatani H F, Yu W, Ritchie R. *Scripta Metall.*, 1988, 22: 93
- [13] Dew Hughes D, Creed E, Miller W S. *Mater Sci. Technol*, 1988, 4: 106
- [14] Jata K V, Starke Jr E A. *Scripta Metall.*, 1988, 22: 1553
- [15] Niinomi N, Degawa K, Kobayashi T. *In: Champier G, Dubost B, Minannay D, Sabetay L. Aluminum-Lithium Alloys IV. Journal de Physique, Paris, 1987. 653*
- [16] Webster D. *In: Baker C, Gregson P J, Harris S J, Peel C J. Aluminum-Lithium Alloys III. The Institute of Metals, London, 1986. 602*
- [17] Welpmann K, Lee Y T, Peters M. *In: Sanders Jr T H, Starke Jr E A. Aluminum-Lithium Alloys V. Williamsburg, Virginia, 1989. 1513*
- [18] Yao D P, Hu Z Q, Li Y Y, Shi C X. *Chin J. Met. Sci. Technol*, 1990, 6: 31
- [19] Bulmuth E S. *Scripta Metall.*, 1984, 18: 301
- [20] Mereau C, Allouche A, Knystantas E J J. *Appl. Phys.*, 1985, 58: 4582
- [21] Jiang X J. Master Degree Dissertation, Inst., of Metal Research, Academia Sinica, 1990
- [22] Yao D P, Hu Z Q, Li Y Y, Zhang Y, Shi C X. *Acta Metall. Sinica*, 1990, 26: 341
- [23] Ceresara S, Giarada A, Sanchez A. *Phil. Mag.*, 1977, 35: 97
- [24] Yao D P, Zhang Y, Hu Z Q, Li Y Y, Shi C X. *Scripta Metall.*, 1989, 23: 537
- [25] Yao D P, Hu Z Q, Zhang Y, Shi C X. *Acta Metall. Sinica*, 1990, 26: A122
- [26] Yao D P, Hu Z Q, Li Y Y, Zhang Y, Shi C X. *Mater. Sci. Prog*, 1990, 4: 409
- [27] Yao D P, Zhang Y, Hu Z Q, Li Y Y, Shi C X. *Acta Metall. Sinica*, 1988, 24(Sapple II): SA98
- [28] Yao D P, Hu Z Q, Li Y Y, Zhang Y, Shi C X, *Acta Metall. Sinica*, 1990, 26: A97
- [29] Zhang Y, Zhao H E, Guo G Z, Chen J Z, Yao D P, Hu Z Q. *In: Sanders Jr T H, Starke Jr E A, Starke Jr E A. Aluminum-Lithium Alloys V. Williamsburg, Virginia, 1989, 539*
- [30] Yao D P, Li Y Y, Hu Z Q, Zhang Y, and Shi C X. *Mater. Res. Prog.* 1990, 4: 309
- [31] Glazer J, Morris Jr J W. *In: Sanders Jr T H, Starke Jr E A. Aluminum-Lithium Alloys V. Williamsburg, Virginia, 1989, 1471*
- [32] Ral K T V, Yu W, Ritchie R O. *Metall. Trans. A*, 1989, 20A: 485

- [33] Rao K T V, Ritchie R O. *In: Sanders Jr T H, Starke Jr E A. Aluminum-Lithium Alloys V. Williamsburg, Virginia, 1989, 1501*
- [34] Yao D P, Hu Z Q, Li Y Y, Zhang Y, Shi C X. *Chin. J. Met. Sci. Technol.*, 1990, 6: 277
- [35] Yao D P, Hu Z Q, Li Y Y, Zhang Y, Shi C X. unpublished paper
- [36] Yao D P, Hu Z Q, Li Y Y, Zhang Y, Shi C X. *In: Sanders Jr T H, Starke Jr E A. Aluminum-Lithium Alloys V. Williamsburg, Virginia, 1989. 1533*
- [37] Yao D P, Hu Z Q, Li Y Y, Zhang Y, Shi C X. *Acta Metall. Sin. (Eng. Ed)*, 1990, 3: 302
- [38] Xu Y B, Wang Z G, Zhang Y, Zhao H H, Hu Z Q. *In: Sanders Jr T H, Starke Jr E A. Aluminum-Lithium Alloys V. Williamsburg, Virginia, 1989. 1147*
- [39] Vaudevan A K, Doherty R D. *Acta Metall*, 1987, 35: 1193
- [40] Xu Y B, Wang L, Zhang Y, Wang Z G, Hu Z Q. *Metall. Trans.*, 1991, A22: 723
- [41] Wu Y. private communication
- [42] Mang W S, Wang G Z, Zhang Y C, Hu Z Q, Shi C X. *Acta Metall. Sinica*, 1990, 26: A8
- [43] Zhang Y C, Wu Y, Hao Y Y, Liu Z G, Chen G Y. *In: Sanders Jr T H, Starke Jr E A. Aluminum-Lithium Alloys V. Williamsburg, Virginia, 1989. 95*
- [44] Miyami Y, Hino M, Eto T. *Light Metals*, 1986, 36: 697
- [45] Quist W E, Narayanan G H, Wingert A L, Rouald T M. *In: Baker C, Gregson P J, Harris S J, Peel C J. Aluminum-Lithium Alloys. the Inst. of Met-als, London, 1986. 625*
- [46] Kojima K A, Lewis R E, Kaufman M J. *In: Sanders Jr T H, Starke Jr E A. Aluminum-Lithium Alloys V. Williamsburg, Virginia, 1989. 85*
- [47] Yao D P, Hu Z Q, Li Y Y, Zhang Y, Shi C X. *In: Sanders Jr T H, Starke Jr E A. Aluminum-Lithium Alloys V. Williamsburg, Virginia, 1989. 105*